Materials Science Forum Vols. 269-272 (1998) pp. 837-842

MECHANICAL AND CORROSION BEHAVIOUR OF Al-Fe-Nb AMORPHOUS ALLOYS

F. Audebert[1], S. Vázquez[1], A. Gutiérrez[2], I. Vergara[3], G. Alvarez[4], A. García Escorial[2] and H. Sirkin[1].

[1] Laboratorio de Sólidos Amorfos, Facultad de Ingeniería, Universidad de Buenos Aires, Paseo Colón 850, (1063) Buenos Aires, Argentina.

[2] CENIM-CSIC, Av. Gregorio del Amo 8, (28040) Madrid, España.

[3] Dpto. Física Aplicada, E. P. S., Universidad Carlos III de Madrid, C/ Butarque 15, (28911) Leganés, Madrid, España.

[4] U.A. Materiales, C.A.C., Comisión Nacional de Energía Atómica, Av. del Libertador 8250, (1429) Buenos Aires, Argentina.

Keywords: Aluminium Amorphous Alloys, Mechanical Properties, Corrosion Behaviour, X ray Photoelectron Spectroscopy (XPS).

Abstract

The development of new nanostructured and amorphous Al-alloys gives much hope to develop new improved light materials with high specific strengths and good corrosion resistance.

In a previous work [1], the amorphicity range in Al-rich Al-Fe-Nb alloys produced by the melt-spinning technique was determined.

In this work, the mechanical and corrosion behaviour of these alloys in the amorphous and partially amorphous states, is reported.

The mechanical characterisation was carried out by microhardness and nanoindentation tests, the latter in order to determine Young's modulus.

The corrosion behaviour has been evaluated by means of potentiodynamic polarisation techniques in a chloride containing solution. Results have been compared with those obtained for crystalline alloys with the same chemical composition. X-ray photoelectron spectroscopy (XPS) has been used to analyse the oxide film formed in melt-spun samples during the rapid quenching under air atmosphere.

The Al-Fe-Nb fully amorphous alloys exhibit low Young`s moduli, high microhardness values and a good corrosion behaviour.

1. Introduction

High performance aluminium alloys have been the object of intensive research in the past few years. Research efforts have been concentrated on the development of new alloys with different chemical compositions and novel processing techniques with capability to produce structures with outstanding properties. Rapid Solidification (RS) processing has played a major role in recent developments in this field, because it produces a general refinement of the microstructure, extension of the solid solubility and the formation of metastable phases (crystallines, amorphous and quasicrystals) [2,3]. Such microstructural modifications often produces an improvement of the properties, as the wear and corrosion resistance.

In the last years, the mechanical properties of the Al Amorphous Alloys (AAA), have been the subject of several works [4,5]. On the other hand, some works have focused on the corrosion behaviour of Al alloys obtained by RS [6,7]; only in few cases the mechanical and corrosion behaviour of RS Al alloys, have been studied [8].

One potential technological applications of AAA is their use as a protective coating or surface resistant to wear and corrosion. Then, it is interesting to characterise the mechanical and corrosion behaviour of the Al-Fe-Nb amorphous alloys.

In previous works [1,9,10], the glass forming ability, the atomic structure and crystallisation process of melt-spun Al-Fe-Nb alloys had been studied. In this work, the microhardness values and the Young's modulus are determined. Additionally, the electrochemical corrosion behaviour of the $Al_{87}Fe_{10}Nb_3$ amorphous alloy, that showed the best combination of the hardness and elasticity for the wear resistance, was studied by means of potentiodynamic polarisation techniques. Also, the oxide film formed in a melt-spun amorphous sample during the RS under air atmosphere was characterised by XPS.

2. Experimental

The melt spun samples used by this work were produced under air atmosphere as described in [1]. The composition of the studied alloys and their structure in as-quenched state, as determined by X ray diffraction and differential scanning calorimetry are shown in Table 1.

Microhardness measurements were performed on both sides of the ribbons using a Shimadzu HV-2000 microhardness tester with a Vickers indenter at a load of 50 gf during 15 sec.

The nanoindentation test was carried out by means of a Nanoindenter IIs Tester (Nano Instruments Inc., Knoxville, Tn). A Berkovich indenter, a three-sided pyramid with an area-to-depth function which is the same as that of a Vickers indenter, was used. Then in this test is possible to measure a hardness value, the nanohardness, and to compare against the Vickers microhardness. The specimens were mounted in cold-mount epoxy and polished with metallographic techniques. Young's moduli were determined on the indentation unloading in the constant displacement rate test.

The electrochemical behaviour of A-2 amorphous samples was examined by potentiodynamic polarisation measurements in a deaerated 1M-NaCl solution at room temperature, with a scan rate of 0.5 mV/s. The specimens were allowed to reach a stationary open circuit potential during 1 h. Then, the potentiodynamic scan was initiated at a potential value 100 mV lower than the corrosion potential. In order to compare the behaviour of the A-2 amorphous alloys with that of their crystalline counterparts, samples in the crystallised state were prepared by annealing for 5 h at 775 K in vacuum.

XPS spectra of the A-2 melt-spun amorphous samples were recorded under ultra-high vaccum (UHV) conditions with a commercial VG-CLAM hemispherical electron energy analyser. The excitation energy was Mg Kα. The base pressure in the UHV-chamber during measurements was better than 10^{-9} mbar. An ion sputtering gun, operated at 3 Kev, was used to obtain the in-depth distribution of species in the oxide film formed on the surface during the RS under air atmosphere.

3. Results and Discussion

3.1 *Mechanical Behaviour*

In Table 1 are listed the results of the microhardness and the nanoindentation tests, in form of average values with their corresponding standard deviation.

Microhardness values on both sides of the ribbons do not show appreciable differences. Therefore, to determine the average microhardness value, the better indentations of both sides of the ribbons were considered.

The nanoindenter test needs a good polished surface and a homogeneous microstructure. Due to the last condition it was not possible to measure on the A-5 alloys because it contains a high crystalline fraction. Young's moduli determinations are more sensitive to the microstructural inhomogenity than the nanohardness values, as can be observed in the standard deviation of the A-3 and A-4 alloys.

The difference between microhardness and nanohardness values is around 1.5 GPa, similar to that reported in the Metglass 2826, [11].

Table 1: Alloy Composition (at. %), as-quenched structure [10], Vickers microhardness (Hv50), nanohardness (Hdnm) and Young's modulus (E) for the different studied alloys.

Alloys	**A-1**	**A-2**	**A-3**	**A-4**	**A-5**
Composition	$Al_{90}Fe_7Nb_3$	$Al_{87}Fe_{10}Nb_3$	$Al_{87}Fe_8Nb_5$	$Al_{84}Fe_{13}Nb_3$	$Al_{80}Fe_{10}Nb_{10}$
Structure	Amorphous	Amorphous	Amorphous*	PC (40-45 %)	PC (15-20 %)
Hv50 [GPa]	3.0 ± 0.2	4.2 ± 0.2	4.7 ± 0.2	5.7 ± 0.3	5.5 ± 0.6
Hdnm [GPa]	4.7 ± 0.4	5.5 ± 0.1	6.3 ± 0.1	6.9 ± 0.5	---
E [GPa]	40 ± 2	41 ± 3	85 ± 10	105 ± 11	---

Amorphous*: with an undetermined small fraction of crystalline phases.

PC: Partially Crystalline (amorphous phase fraction in %).

The hardness of these RS Al-alloys is higher than the hardness of the heat treatable commercial aluminium alloys, [12]. Moreover, the microhardness values presented by these Al-Fe-Nb amorphous alloys are as high as those obtained in the Al crystalline alloys hardened by a fine dispersion of icosahedral phases (i-phases), [13]. Then, is possible that the high hardness of Al-Fe-Nb amorphous phase could correspond to a short range order (SRO) similar to the SRO of the Al-Fe-X quasicrystalline phases, as is suggested in ref. [9].

Young's moduli were determined by means of the slope of the unloading curve in the nanoindentation tests, using the following equations:

$$dh/dP = 1/2.h_p.(\pi/24.5)^{1/2}.1/E_r \qquad \text{(i)}$$

$$E_r = (1-\upsilon^2)/E + (1-\upsilon_o^2)/E_o \qquad \text{(ii)}$$

Where, *dh/dP* is the reciprocal of the unloading slope, or the compliance; h_p, is the plastic depth; υ_o, E_o, are the Poisson's ratio and the Young's modulus for the nanoindenter respectively; υ, E, are the same parameters for the sample.

In the calculations of the E values, a Poisson's ratio of $\upsilon = 0.33$, identical to the Al crystalline alloys, was adopted [12].

The Young's moduli corresonding to A-1 and A-2 amorphous alloys are lower than the pure Al and Al commercial alloys ($E \cong 70$ Gpa.), but they are similar to those reported for Al-Fe-Gd amorphous and partially amorphous alloys [14]. The A-3 and A-4 alloys presents E values higher than pure Al, and similar to some quasicrystalline alloys [15].

A good wear resistant coating may need a higher hardness and a higher elasticity than the bulk materials to avoid the superficial crack formation. Both A-1 and A-2 alloys exhibit these conditions respect to the Al commercial alloys.

3.2 *Corrosion Behaviour*

The A-2 amorphous alloy presents better properties than the A-1 amorphous alloy to be used as a wear resistant coating. Then we have selected this alloy to study the electrochemical corrosion behaviour.

Figure 1 shows the polarisation curves for the A-2 alloy in both amorphous and crystallised states and for the pure Al (99,99 %), in a 1M-NaCl solution. The three samples present a similar behaviour. The open circuit potential of the $Al_{87}Fe_{10}Nb_3$ alloy has a similar value to that corresponding to pure Al, [16].

Upon increasing the potential above the corrosion potential, all curves showed a passive zone. The passive current density of the as-spun amorphous alloy is 10^{-6} A/cm^2, one order of magnitude lower than those shown by the pure Al and the crystallised sample. In order to characterise the "active state" of the amorphous alloys, the oxide films formed during quenching, in the Melt Spinning process, were chemically removed using a NaOH at 2.5 % solution. Then, the amorphous alloys in the active state present a higher

passive current density similar to the crystalline samples.

When the potential is further increased, there is a critical potential value above which the current increases sharply. This potential at which the passivity breaks down is called the pitting potential. The microscopical examination of the samples after the polarisation test revealed the pitting process. The amorphous alloy in both "passive" (with the as-spun oxide film) and active states presents the same pitting potential value, at around 0.15 V(she) (standard hydrogen electrode).

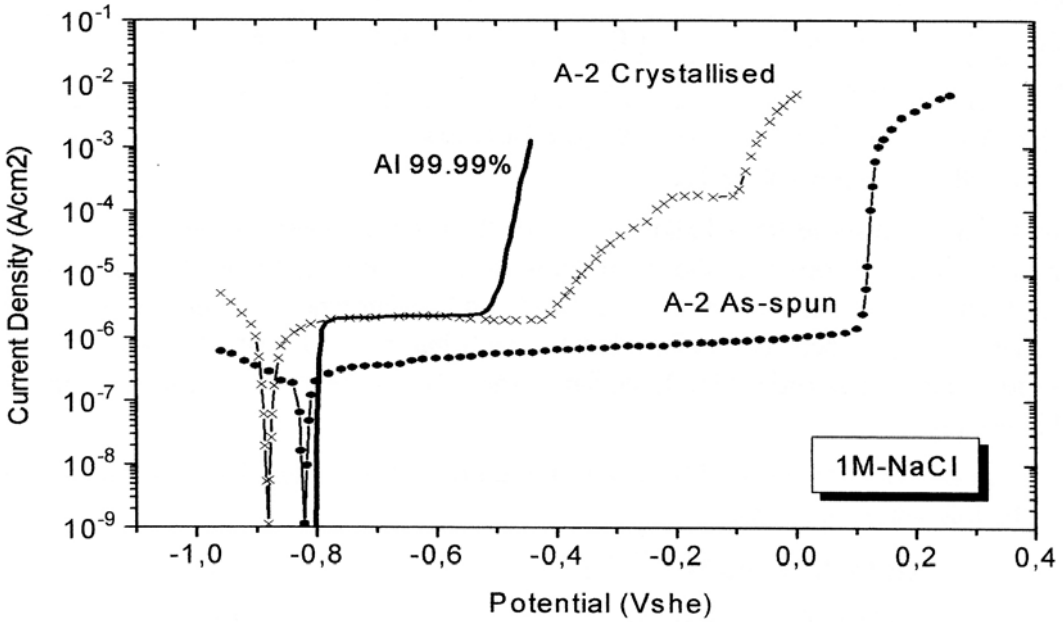

Figure 1: Polarisation curves of the A-2 alloy in both amorphous and crystallised states and of the pure Al (99.99%), in a 1M-NaCl solution.

The pitting potential of pure Al in a 1M-NaCl solution is -0.55 V(she), [16]. The polarisation curve of the crystallised sample shows a passivity breakdown at a value 100 mV higher than for pure Al.

On the other hand, the anodic polarisation curve of the A-2 amorphous alloy presents a strong ennoblement of the pitting potential respect to the A-2 crystallised alloy about of 500-550 mV.

Yoshioka [8] did not found a effective enhancement of the pitting corrosion resistance on Al-Fe alloys neither with slow or rapid solidification. Whereas, on RS Al-Si-Nb crystalline alloys an important increase of the pitting potential has been observed. They attributed this ennoblement of the pitting potential and the enhancement of corrosion resistance to the supersaturation of α-Al phase and to the elimination or decrease of the Si and intermetallic phases responsible for pitting corrosion.

Accordingly, the sluggish enhancement of the pitting corrosion resistance of the A-2 crystallised alloy can be attributed to the presence of the Nb. Whereas, the higher ennoblement of the pitting potential on the AAA alloyed with Nb, was also reported by Yoshioka [7] on the sputter deposited Al-Nb amorphous alloys, polarised in 1M-HCl solution.

The Al-Fe-Nb amorphous alloys can be considered chemically as a single solution phase, similar to a single α-Al supersaturated phase. Then is reasonable that these amorphous alloys have an enhancement of pitting corrosion resistance because, as it is known, the corrosion attack of conventionally Al cast alloys takes place preferentially in the α-Al phase adjacent to the silicon and/or intermetallic compound.

On the other hand, the oxide film formed during the RS is the real superficial layer that interacts with the environment. Consequently, is very important to characterise this layer and to analyse its protection ability. The potentiodynamic polarisation curves revealed that this oxide film decreases the passive current density but does not produce any effect on the pitting potential, with respect to the $Al_{87}Fe_{10}Nb_3$ amorphous alloy in the active state.

In order to characterise this oxide film, a XPS analysis on both ribbon sides were carried out.

Figure 2, shows the in-depth distribution of the different chemical species of the O, Al, Fe and Nb measured on the ribbon side that quenched in air contact, "air side" (AS), represented by the intensity of XPS spectra as a function of the sputtering time, which is proportional to the depth (2 μA min ≈ 1 nm).

Both ribbon sides, the AS and that one quenched on the wheel (WS) present a similar in-depth distribution. In figure 2, can be distinguished two layers. The most external layer with a thickness between 10 and 15 nm is mainly composed of $Al(OH)_3$, with some amount of Al_2O_3, and very small fraction of Fe and Nb. Below this layer, both Al^{3+} and OH^- signals sharply decrease, whereas those of metallic Al, Fe and Nb increase and the O^{2-} signal almost disappears.

The internal layer is much thicker and is characterised by a remainder amount of $Al(OH)_3$ and a continuous increase of metallic Al, Fe and Nb. Both Al and Fe reach a saturation concentration before the maximum depth probed, 60 nm, whereas Nb seems to further increase below this depth.

The result observed on the external layer is in agreement with that reported by Yoshioka [17] on the oxide film with a thickness of 2-3 nm, formed on sputter deposited Al-Nb amorphous alloys. Although the concentration of Fe and Nb species gradually increases with depth, this is not sufficient to avoid the pitting corrosion of the Al-Fe-Nb amorphous alloys in 1M-NaCl solution, but is probably the reason of the enhancement of the pitting corrosion resistance respect to the pure Al and the crystallised Al-Fe-Nb alloy.

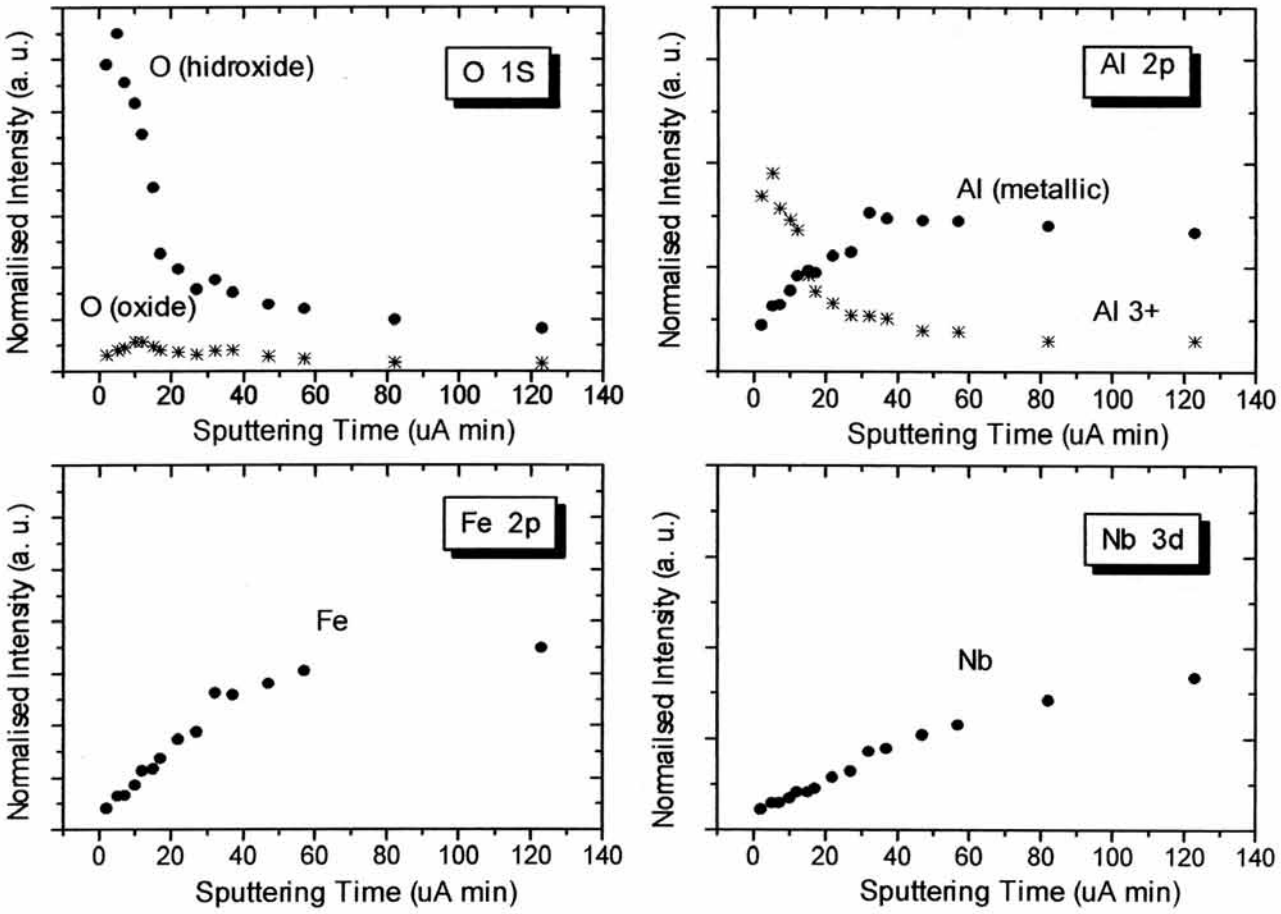

Figure 2: Intensity of the XPS spectra of the O-1S, Al-2p, Fe-2p and Nb-3d binding energy as a function of the sputtering time, measured on the "air side" of the ribbon of the A-2 alloy.

4. Conclusions

The hardness of the Al-Fe-Nb amorphous alloys is higher than the hardness of the heat treatable

commercial aluminium alloys and is as high as those obtained in the Al crystalline alloys hardened by a fine dispersion of i-phases. This fact can be attributed to the short range order (SRO) of the Al-Fe-Nb amorphous phase similar to the SRO of the Al-Fe-X quasicrystalline phases, as is suggested in [9].

The Young's moduli of the Al-Fe-Nb fully amorphous alloys are around a 40% lower than the corresponding to Al metal.

The $Al_{87}Fe_{10}Nb_3$ amorphous alloy is spontaneously passivated in 1M-NaCl solution and it is susceptible to passivity breakdown by anodic polarisation, but presents a strong ennoblement of the pitting potential of about 650 mV respect to Al metal and and 550 mV respect to crystallised alloy.

The oxide film formed during the RS on the $A_{l87}Fe_{10}Nb_3$ amorphous alloy is very similar on both ribbon sides, being much thicker on the "air side". The film is characterised by two different layers, the external layer is composed mainly of $Al(OH)_3$ and the internal layer contains a remainder amount of $Al(OH)_3$ and is gradually enriched with metallic Al, Fe and Nb. This oxide film of the as-spun ribbons is the responsible of the lower passive current density with respect to "active alloy", but does not produce any effect on the pitting potential.

Thus, the mechanical and corrosion characterisation of Al-Fe-Nb amorphous alloys suggests that these amorphous phases can be good candidates to be used as wear and corrosion resistant coating.

5. Acknowledgements

This work was financially supported by CICYT MAT95-0796 and UBA IN-052.

6. References

[1] F. Audebert, H. Sirkin and A. García Escorial, Scrip. Mat. 36 (1997), p. 405.

[2] S.K. Das, R.L. Bye and P.S. Gilman, Mater. Sci. and Eng. A-134 (1991), p. 1103.

[3] A. Inoue, NanoStructured Mat. 6 (1995), p. 53.

[4] Y. He, G.M. Dougherty, G.J. Shiflet and S.J. Poon, Acta Metall. Mater. 41 (1993), p. 337.

[5] T. Masumoto, Mater. Sci. and Eng. A-179/180 (1994), p. 8.

[6] R. Li, M. Ferreira, A. Almeida, R. Vilar, K. Watkins, M. McMahon and W. Steen, Surface & Coat. Tech. 81 (1996), p. 290.

[7] H. Yoshioka, Q, Yan, H. Habazaqui, A. Kawashima, K. Asami and K. Hashimoto, Corr. Sci. 31 (1990), p. 349.

[8] H. Yoshioka, S. Yoshida, A. Kawashima, K. Asami and K. Hashimoto, Corr. Sci. 26 (1986), p. 795.

[9] F. Audebert, H. Sirkin and A. García Escorial, Phil. Mag. B, (1997), in press.

[10] F. Audebert, H. Sirkin and A. García Escorial, Proc. of "V Workshop on Non-Cryst. Solids", Word Scientific Publishing Co., (1997), in press.

[11] M.F. Doermer,."Mechanical Properties of Metallic Thin Films on Substrates Using Sub-Micron Indentation Methods and Thin Film Stress Measurement Techniques", Ph.D.Thesis, Stanford University, (1987), p. 111.

[12] "Aluminum and Aluminum Alloys", ASM Specialty Handbook, ed.: J.R. Davis, USA, (1993).

[13] A. Inoue, M. Watanabe, H. Kimura, F. Takahashi, A. Nagata and T. Masumoto, Mater. Trans., JIM 33 (1992), p. 723.

[14] G.J. Shiflet, Y. He and S.J. Poon, Scrip. Metall. 22 (1988), p. 1661.

[15] J.M. Dubois, "Trends in Non-Crystalline Solids", Word Scientific, (1991), p. 343.

[16] J.R. Galvele and S.M. de De Micheli, Corr. Sci. 10 (1970), p. 795.

[17] H. Yoshioka, A. Kawasima, K. Asami and K. Hashimoto, "Proc. Symp. Corrosion, Electrochemistry and Catalysis of Metallic Glasses", The Electrochemical Society, Pennington, (1988), p. 242.

Corresponding Author: Fernando Audebert, e-mail: faudebe@aleph.fi.uba.ar / Fax: (54-1) 331-1852.